

## Thickness inhomogeneities in the organometallic chemical vapor deposition of GaP

X. Liu and D. E. Aspnes

Citation: [Applied Physics Letters](#) **93**, 203104 (2008); doi: 10.1063/1.3029742

View online: <http://dx.doi.org/10.1063/1.3029742>

View Table of Contents: <http://scitation.aip.org/content/aip/journal/apl/93/20?ver=pdfcov>

Published by the [AIP Publishing](#)

---

### Articles you may be interested in

[Lattice-engineered Si<sub>1-x</sub>Gex-buffer on Si\(001\) for GaP integration](#)

[J. Appl. Phys.](#) **115**, 103501 (2014); 10.1063/1.4864777

[Structural and optical properties of GaInP grown on germanium by metal-organic chemical vapor deposition](#)

[Appl. Phys. Lett.](#) **97**, 121909 (2010); 10.1063/1.3492854

[Thickness inhomogeneities and growth mechanisms of GaP heteroepitaxy by organometallic chemical vapor deposition](#)

[J. Vac. Sci. Technol. A](#) **28**, 583 (2010); 10.1116/1.3442805

[Erratum: "Elimination of nonuniformities in thick GaN films using metalorganic chemical vapor deposited GaN templates" \[\[J. Appl. Phys.\]\(#\) \*\*90\*\*, 6011 \(2001\)\]](#)

[J. Appl. Phys.](#) **91**, 6778 (2002); 10.1063/1.1471940

[Elimination of nonuniformities in thick GaN films using metalorganic chemical vapor deposited GaN templates](#)

[J. Appl. Phys.](#) **90**, 6011 (2001); 10.1063/1.1415363

---

Confidently measure down to 0.01 fA and up to 10 PΩ  
Keysight B2980A Series Picoammeters/Electrometers

[View video demo](#)





# Thickness inhomogeneities in the organometallic chemical vapor deposition of GaP

X. Liu<sup>a)</sup> and D. E. Aspnes

Department of Physics, North Carolina State University, Raleigh, North Carolina 27695-8202, USA

(Received 24 October 2008; accepted 30 October 2008; published online 18 November 2008)

We analyze exponential lateral-thickness variations observed in the growth of GaP on (001) GaAs, thermally generated SiO<sub>2</sub>, (001) Si, and nanoscopically roughened Si surfaces by organometallic chemical vapor deposition, using as a reference the polycrystalline GaP deposited on the Mo susceptor surrounding the 2 in. wafers. We find these variations to be due to differences in the chemical reactivities of the various surfaces toward the generation of a precursor, probably a H–P=Ga–CH<sub>3</sub> dimer adduct, by heterogeneous catalysis followed by desorption and diffusion through the gas phase. © 2008 American Institute of Physics. [DOI: 10.1063/1.3029742]

Lateral thickness inhomogeneities are commonly observed for films deposited by organometallic chemical vapor deposition (OMCVD) for a wide range of reactor configurations such as vertical,<sup>1–4</sup> pancake,<sup>5</sup> and horizontal.<sup>6–12</sup> Extensive experimental studies<sup>1,4,6,7,9,12</sup> and numerical simulations<sup>2–6,8,10–12</sup> of this topic exist for the epitaxial growth of GaAs,<sup>1,2,6–9,11</sup> GaN,<sup>4,12</sup> and Si.<sup>3,5,10</sup> These inhomogeneities are generally ascribed to depletion of gas-phase reactants,<sup>6,10,12</sup> parasitic deposition,<sup>1,9,11</sup> variation of the thicknesses of diffusion-boundary layers,<sup>1,5,7</sup> gas-flow characteristics,<sup>2,8</sup> thermal effects,<sup>3,10</sup> and rate limiting by mass transport as opposed to diffusion<sup>1</sup> or surface kinetics.<sup>5</sup>

More interesting are the systematic variations that occur near sample peripheries. Hemmingsson *et al.*<sup>4</sup> and Dam *et al.*<sup>12</sup> found the growth rate at the edge of wafers in GaN homoepitaxy to be higher than that at the center. They attributed this to lateral back diffusion of GaCl from the area surrounding the substrate, assuming lower depletion by the polycrystalline GaN deposited there. Similar effects have been reported in the selective-area growth of GaN,<sup>13–15</sup> where a higher edge growth rate was again ascribed to back diffusion of reactants from the mask regions. This diffusion process was verified by Mitchell *et al.*<sup>15</sup> to occur primarily in the gas phase.

Here, we report comparative studies of edge effects for GaP deposited by OMCVD on (001)GaAs, thermally gener-

ated SiO<sub>2</sub>, (001)Si, nanoscopically roughened (nr) Si, and the polycrystalline GaP deposited on the molybdenum (Mo) susceptor surrounding the 2 in. diameter wafers, showing that information about growth mechanisms can be obtained as well. We describe analytically the exponential lateral variations that we observe by solving a one-dimensional (1D) diffusion equation. The data are consistent with a growth process where a precursor, probably a H–P=Ga–CH<sub>3</sub> dimer adduct, is formed by heterogeneous catalysis, mainly desorbs, then—consistent with the studies mentioned above—diffuses in the gas phase.

The OMCVD reactor is a modified Emcore model GS3300 of shower-head, cold-wall, and rotating-disk design. Growth was done with trimethylgallium (TMG) and phosphine (PH<sub>3</sub>) sources at a chamber pressure of 4 Torr to enhance diffusion. The 2 in. diameter substrates were placed in the slightly recessed central region of a 3 in. diameter Mo susceptor, so the samples are surrounded by a Mo ring that is 0.5 in. wide. Prior to loading, the (001)GaAs substrates were given a 10% HCl rinse. The as-polished (001)Si substrates were given a standard RCA clean plus a final 10% HF rinse. The SiO<sub>2</sub> substrates of root mean square (rms) roughness less than 0.5 nm were generated *in situ* by first heating the Si substrates to 800 °C under H<sub>2</sub> flow, then exposing the surface six times to O<sub>2</sub> bursts of 2 s each. Two types of nrSi substrates were used. The first, denoted nrSi(NH<sub>4</sub>F),

TABLE I. Growth conditions and thickness variations for the representative depositions.

Run	Subs.	Gas	$\omega$ (rpm)	$T(^{\circ}\text{C})$	V/III	$F_{\text{TMG}}$ (sccm)	$G_C$ (nm/s)	$T_E$ (nm) <sup>c</sup>
A	GaAs	H <sub>2</sub>	1200	570	3300	0.52	0.15	$75-0.3e^{x/5.5}$
B	GaAs	H <sub>2</sub>	0	580	530	0.38	0.06	$134-0.5e^{x/6.0}$
C	SiO <sub>2</sub>	H <sub>2</sub>	1200	570	400 <sup>a</sup>	0.25	0.09	$255-2.8 \times 10^{-9} e^{x/1.1}$
D	SiO <sub>2</sub>	N <sub>2</sub>	1200	600	6200 <sup>a</sup>	0.52 <sup>a</sup>	0.17	$302-0.07x$
E	Si	N <sub>2</sub>	0	550	6300	0.63	N/A	N/A
F	nrSi(NH <sub>4</sub> F)	N <sub>2</sub>	0	680	2400	0.34	N/A	N/A
G	nrSi(1:1:1)	N <sub>2</sub>	0	600	2700	0.91	0.21 <sup>b</sup>	$107+0.3e^{x/5.0}$

<sup>a</sup>Stabilized value.<sup>b</sup>Determined from  $T_E$  divided over time rather than real-time spectroscopic polarimetry.<sup>c</sup>Units of  $x$  are mm.<sup>a)</sup>Author to whom correspondence should be addressed. Electronic mail: xliu.ncsu@gmail.com.

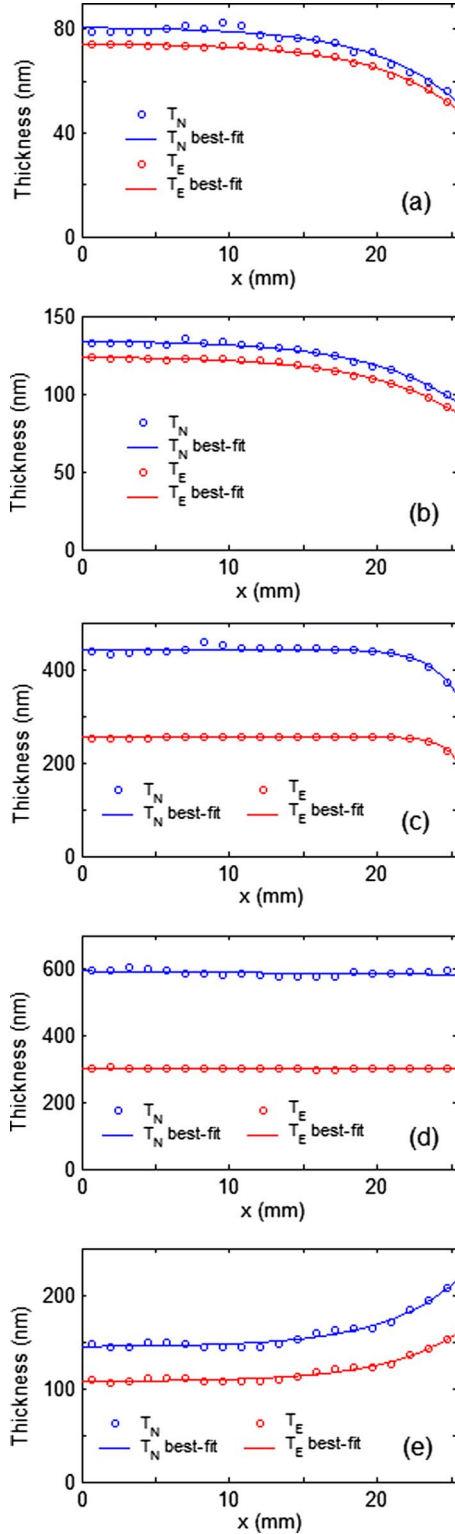


FIG. 1. (Color online) (a)–(e) Nominal (blue) and effective (red) lateral thicknesses together with best-fit exponential dependences for depositions A (a), B (b), C (c), D (d), and G (e), which are defined in Table I.

was generated by etching in a 10%  $\text{NH}_4\text{F}$  solution at 80 °C for 2 to 7 min. This process is very slow, being anisotropic and reaction-rate limited,<sup>16</sup> leaving a surface that is fairly rough (10 nm rms) but with a low density of kink sites. The second, denoted nrSi(1:1:1), was generated by etching with  $\text{HF}:\text{HNO}_3:\text{H}_2\text{O}=1:1:1$  at room temperature for 10 to 30 s. For this composition, the process is rapid, isotropic, and diffusion limited,<sup>17</sup> leaving a surface of rms roughness of about 5 nm with a high density of kink sites.

Conditions for the seven representative depositions analyzed in detail here are summarized in Table I. Kinematics calculations show that in all cases, growth occurred under diffusion-limited conditions. Thickness profiles were determined after growth by four-phase-model analysis of 20 pseudodielectric-function  $\langle\epsilon\rangle$  spectra taken per sample by spectroscopic ellipsometry at evenly spaced intervals across the 1 in. radius. Results are expressed in Fig. 1 as an effective thickness  $T_E=(\text{bulk thickness}\times\text{bulk concentration}+\text{top thickness}\times\text{top concentration})$  and a nominal thickness  $T_N$ . Figure 1 also show the best-fit exponentials for depositions A–D and G. Here,  $x=0$  and 25.4 mm represent the center and edge of the wafer, respectively. Table I also provides the numerical forms of  $T_E$  and the growth rates at the film centers for all depositions except E and F, which were done on substrates that favor growth of three-dimensional islands. For those that can be analyzed, the films are either thinner (A–C) or thicker (G) at the edges than at the center, but all show an exponential dependence on radius.

We model the thickness inhomogeneities as follows. We suppose that the inhomogeneities are due to lateral diffusion and derive the analytic form of a general concentration  $n(x)$  from the 1D continuity equation

$$\nabla \cdot \mathbf{J} + \frac{\partial n}{\partial t} = g_n - r_n. \quad (1)$$

Here  $\mathbf{J}=-D(\partial n/\partial x)\hat{x}$  is the mass-transport current and  $g_n$  and  $r_n$  are the generation and removal rates of the active species, respectively. In steady state  $\partial n/\partial t=0$ . A 1D treatment is acceptable if the characteristic length of the thickness variation is small compared to the substrate radius, as is the case here. In our system, diffusion can only occur in the gas phase since a gap between the sample and the outer ring of the susceptor prevents diffusion over the surface. We assume that the active species is removed by decomposition, deposition, and/or diffusion normal to the surface, which together act to yield Poisson statistics with time constant  $\tau$ . With these assumptions, Eq. (1) becomes

$$-D\frac{\partial^2 n}{\partial x^2} = -\frac{n}{\tau} + g_n. \quad (2)$$

This can be solved using the Green-function approach. We obtain

$$n(x) = \int dx_0 G(x, x_0) g_n, \quad (3)$$

where  $G(x, x_0)=L/2De^{-|x-x_0|/L}$  with a characteristic diffusion length  $L=\sqrt{D\tau}$ . If  $g_n$  is a constant  $n_0$ , then  $n(x)=n_0L^2/D$  is also a constant. In this case, deposition is uniform, as in the central regions of the substrates. However, if  $g_n=n_0$  only over a limited range, then Eqs. (2) and (3) give

$$n(x) = \frac{n_0L^2}{D} - \frac{n_0L^2}{2D}e^{(x-a)/L} \quad \text{for } x < a, \quad (4a)$$

and

$$n(x) = \frac{n_0L^2}{2D}e^{-(x-a)/L} \quad \text{for } x > a. \quad (4b)$$

The two solutions join smoothly at  $x=a$ . Thus exponential behavior occurs near the boundaries, with the exponentials increasing or decreasing as the boundary is approached de-

pending on which side the concentration is higher. Generalization to the case of different generation rates and/or multiple regions is straightforward. Equations (4a) and (4b) with adjustable scaling factors for the exponentials were used to calculate the best-fit curves in Fig. 1.

Since the above theory coincides well with the data, we interpret the origin of the thickness inhomogeneities in terms of these expressions. The assumption of gas-phase diffusion appears to contradict the conclusion indicated by the calculated Péclet numbers, which are larger than 1 but smaller than 10. These values imply mass transport primarily by advection. In fact this is what occurs for TMG and  $\text{PH}_3$  and their homogeneous decomposition products. Hence, we conclude that these precursors alone cannot be directly responsible for deposition. Instead, deposition must result from another species, one that involves both Ga and P, is formed by heterogeneous catalysis, largely desorbs, and communicates with different regions via gas-phase diffusion. From the data, it follows that the generation rates of this species are highest for GaAs and the high-quality epitaxial GaP on GaAs, intermediate on  $\text{SiO}_2$  and the polycrystalline GaP deposited on  $\text{SiO}_2$  and Mo, and lowest on Si, nrSi, and the rough GaP deposited on nrSi.

A primary candidate is the  $\text{H}-\text{P}=\text{Ga}-\text{CH}_3$  dimer adduct. The formation of similar adducts has been suggested for OMCVD growth of InP from trimethylindium and  $\text{PH}_3$  sources,<sup>18–20</sup> and of GaAs from TMG and arsine ( $\text{AsH}_3$ ).<sup>21,22</sup> This adduct would be generated through a reaction between decomposition products of TMG and  $\text{PH}_3$ . It would also be likely to decompose in the gas phase, contributing to  $\tau$  in Eq. (2). Since at our growth temperatures  $\text{PH}_3$  decomposition is very inefficient in the gas phase and depends largely on the catalytic activity of the substrate,<sup>18–20</sup> we conclude that it is the rate-limiting step for adduct generation. This is consistent with the relative bond weakening effects exerted on  $\text{PH}_3$  decomposition by various substrates, which from activation-energy measurements<sup>18,23</sup> occur in the sequence III-V (InP) (Ref. 18)  $> \text{SiO}_2$  (Refs. 18 and 23)  $> \text{Si}$ .<sup>23</sup>

The heterogeneous-catalysis/desorption/diffusion process is probably common since similar precursors have also been invoked to explain OMCVD growth of other semicon-

ductors as noted above. Although our measurements were made at a relatively low pressure, higher pressures are expected to affect mainly diffusion lengths and not basic mechanisms. The results also show that different parts of the surface, including the susceptor, are in constant contact with each other during growth.

This work is supported by the Army Research Laboratory under Grant No. W911NF-04-2-0035.

- <sup>1</sup>G. Costrini and J. J. Coleman, *J. Appl. Phys.* **57**, 2249 (1985).
- <sup>2</sup>Y. N. Makarov and A. I. Zhmakin, *J. Cryst. Growth* **94**, 537 (1989).
- <sup>3</sup>C. R. Kleijn, *Thin Solid Films* **365**, 294 (2000).
- <sup>4</sup>C. Hemmingsson, G. Pozina, M. Heuken, B. Schineller, and B. Monemar, *J. Cryst. Growth* **310**, 906 (2008).
- <sup>5</sup>I. Oh, C. G. Takoudis, and G. W. Neudeck, *J. Electrochem. Soc.* **138**, 554 (1991).
- <sup>6</sup>J. van de Ven, G. M. J. Rutten, M. J. Raaijmakers, and L. J. Giling, *J. Cryst. Growth* **76**, 352 (1986).
- <sup>7</sup>M. Sato and M. Suzuki, *J. Electrochem. Soc.* **134**, 1540 (1987).
- <sup>8</sup>R. J. Field, *J. Cryst. Growth* **97**, 739 (1989).
- <sup>9</sup>Y. Li and L. J. Giling, *J. Cryst. Growth* **156**, 177 (1995).
- <sup>10</sup>H. Habuka, *J. Cryst. Growth* **223**, 145 (2001).
- <sup>11</sup>S. Mazumder and S. A. Lowry, *J. Cryst. Growth* **224**, 165 (2001).
- <sup>12</sup>C. E. C. Dam, A. P. Grzegorzczak, P. R. Hageman, R. Dorsman, C. R. Kleijn, and P. K. Larsen, *J. Cryst. Growth* **271**, 192 (2004).
- <sup>13</sup>Y. Kato, S. Kitamura, K. Hiramatsu, and N. Sawaki, *J. Cryst. Growth* **144**, 133 (1994).
- <sup>14</sup>X. Li, A. M. Jones, S. D. Roh, D. A. Turnbull, S. G. Bishop, and J. J. Coleman, *J. Electron. Mater.* **26**, 306 (1997).
- <sup>15</sup>C. C. Mitchell, M. E. Coltrin, and J. Han, *J. Cryst. Growth* **222**, 144 (2001).
- <sup>16</sup>M. A. Hines, *Int. Rev. Phys. Chem.* **20**, 645 (2001).
- <sup>17</sup>A. Schwartz and H. Robbins, *J. Electrochem. Soc.* **123**, 1903 (1976).
- <sup>18</sup>C. A. Larsen, N. I. Buchan, and G. B. Stringfellow, *J. Cryst. Growth* **85**, 148 (1987).
- <sup>19</sup>N. I. Buchan, C. A. Larsen, and G. B. Stringfellow, *Appl. Phys. Lett.* **51**, 1024 (1987).
- <sup>20</sup>N. I. Buchan, C. A. Larsen, and G. B. Stringfellow, *J. Cryst. Growth* **92**, 605 (1988).
- <sup>21</sup>C. A. Larsen, N. I. Buchan, and G. B. Stringfellow, *Appl. Phys. Lett.* **52**, 480 (1988).
- <sup>22</sup>C. A. Larsen, S. H. Li, N. I. Buchan, G. B. Stringfellow, and D. W. Brown, *J. Cryst. Growth* **102**, 126 (1990).
- <sup>23</sup>G. G. Devyatykh, V. M. Kedyarkin, and A. D. Zorin, *Russ. J. Inorg. Chem.* **14**, 1055 (1969).